ACS APPLIED MATERIALS & INTERFACES

Research Article

www.acsami.org

Spontaneous Formation of an Ideal-Like Field-Effect Channel for Decay-Free Polymeric Thin-Film Transistors by Multiple-Scale Phase Separation

Horng-Long Cheng,*[,†] Jr-Wei Lin,[†] Jrjeng Ruan,*[,‡] Chia-Hsien Lin,[†] Fu-Chiao Wu,[†] Wei-Yang Chou,[†] Ching-Hsiang Chen,[§,∥] Chung-Kai Chang,[⊥] and Hwo-Shuenn Sheu[⊥]

[†]Department of Photonics, Advanced Optoelectronic Technology Center, National Cheng Kung University, Tainan 701, Taiwan

[‡]Department of Materials Science and Engineering, National Cheng Kung University, Tainan 701, Taiwan

[§]Graduate Institute of Applied Science and Technology, National Taiwan University of Science and Technology, Taipei, 106, Taiwan

[∥]Protrustech Corporation Limited, Tainan, Taiwan

[⊥]National Synchrotron Radiation Research Center, Hsinchu 30076, Taiwan

Supporting Information

ABSTRACT: We demonstrate semiconducting polymer-based thin-film transistors (PTFTs) with fast switching performance and an uncommon nondecaying feature. These PTFTs based on widely studied poly(3-hexylthiophene) are developed by incorporating the insulating polymer into the active channel and subjecting the compound to specific, spontaneous multiple-scale phase separation (MSPS). An in-depth study is conducted on the interfacial and phase-separated microstructure of the semiconducting/insulating blending active layer and its effect on the electrical characteristics of PTFTs. The polyblends exhibit a confined crystallization behavior with continuously semiconducting crystalline domains between scattered insulator-rich domains. The insulator-rich domains can block leakage current and strengthen the gate control of the channel. A small amount of the insulating polymer penetrates the bottom of the active channel, resulting in effective interface modification. We show specific MSPS morphology of the present blending films to reduce charge trapping effects, enhance charge accumulation, and create a high-seed switching channel. The findings enable us to develop the required morphological conceptual model of the ideal-like field-effect-modulated polymer-based active channel. The polyblend-based PTFTs with MSPS morphology also have promising sensing functions. This study offers an effective approach for overcoming the major drawbacks (instability and poor switching) of PTFTs, thus allowing such transistors to have potential applications.

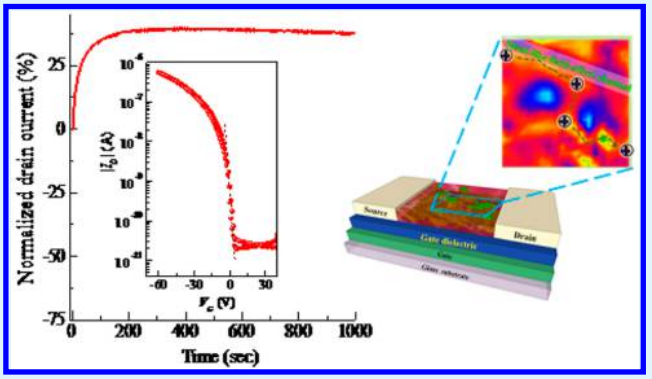

KEYWORDS: *semiconducting-insulating frameworks, polyblends, microstructure−property relationships, thin-film transistors, AFM-Raman spectroscopy, electrostatic force microscopy*

1. INTRODUCTION

Considerable interest has been directed toward organic/polymeric material-based electronics and photonics. Understanding and further controlling microstructural and morphological properties in organic/polymeric materials is essential for their potential applications in various devices because molecular/chain packing is believed to play a key role in determining the charge carrier behaviors within devices and, thus, electrical performance. Compared with vacuum sublimed organic films, polymer thin-films are extremely attractive because of their easy preparation from solution processes and low cost of manufacturing. For electronic devices, polymer thin-films possess unique intrachain and interchain charge transport properties and have superior mechanical and thermal stabilities compared with π-conjugated small molecule semiconductors.[1] These unique advantages make polymer thin-films suitable for potential applications in flexible, lightweight, scalable, and low-cost electronics and photonics.[1−3] However, polymers with long-chain features may result in poorly ordered crystalline, amorphous, and/or aggregate domains and, consequently, complicated microstructure and morphology of the resulting polymer films.[1−5] Meanwhile, the films generally contain a large density of defects and consequently lead to poor and unstable electrical characteristics of electronic devices.[6−13] More recently, significant progress has been made in understanding the charge transport capability [charge mobility values in excess

Received: May 4, 2015
Accepted: July 15, 2015
Published: July 15, 2015

DOI: 10.1021/acsami.5b03864
ACS Appl. Mater. Interfaces 2015, 7, 16486−16494

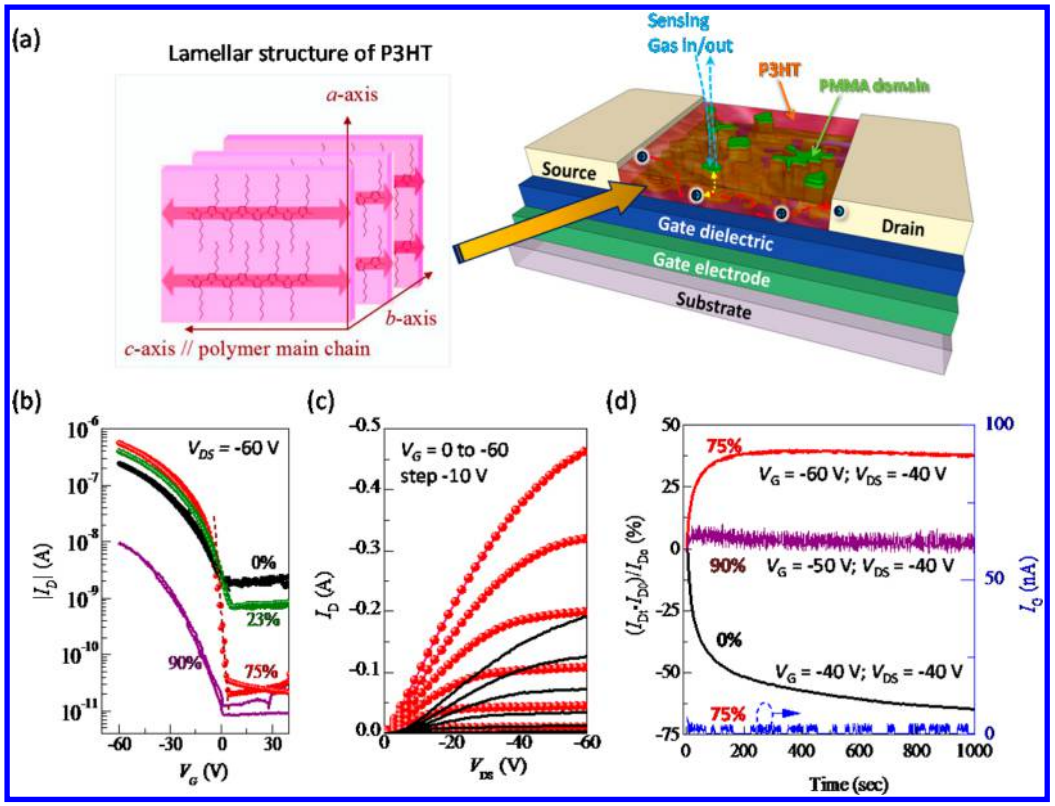

Figure 1. (a) Schematic illustration of the TFT configuration. The lamellar structure of P3HT is shown. (b) Typical transfer curves (drain current, I_D, as a function of gate bias, V_G, at a drain-to-source bias, V_{DS}) of P3HT-based TFTs using various blending active layers. The weight percent of PMMA in the films is shown. (c) Comparison of output curves (I_D as a function of V_{DS} at various V_G) of P3HT-based TFTs with (lines) and without (circles) blending with 75% PMMA as the active layer. (d) Comparison of normalized I_D as a function of time at selected operational conditions. I_{D0} and I_{DT} are the drain current at the initial and at a given time, respectively. The corresponding gate current (I_G) of the 25:75 P3HT/PMMA devices is also shown.

of 1 $cm^2 V^{-1} s^{-1}$, obtained in thin-film transistors (TFTs)][14−16] of conjugated polymers compared with those of π-conjugated small molecule and amorphous silicon TFTs. This breakthrough challenges our understanding of structural-related charge transport properties of polymer films with large disordered areas. However, significant nonideal electrical characteristics could be seen in these polymeric-based TFTs (PTFTs). The major drawback of the use of π-conjugated polymers as the active layer in TFTs is unintentional doping from impurities and/or from oxygen and moisture in ambient air, which leads to an increase in the bulk conductance and results in nonideal electrical characteristics, such as high leakage current in the off-state (I_{off}), transconductance degradation under high gate bias, and poor switch characteristics.[7−11,14−19] Because this concerned unintentional doping mainly occurs in the amorphous regions, further understanding and control of polymeric micro/nanostructure in the active layer of TFTs is desirable for enhancing the stability and unique electrical properties of π-conjugated polymers. However, the requirements for polymeric microstructures in the active channel to achieve PTFTs with ideal field-effect channels are still unclear; these PTFTs are fast switching and produce stable current output under gate modulation and cutoff leakage pathway. A low I_{off} and steep subthreshold swing (S) behavior are important for real electronic applications, particularly with high dynamic performance and low power consumption.

PTFTs always exhibit poor environmental and operational stability, which are the main bottlenecks that hinder their commercial applications. To overcome these limitations, several approaches have been proposed, such as the design and synthesis of new polymers with better MO energy levels against oxidation,[14−16] improvement in molecular packing and ordering of the polymer films,[4,5,20] and protection of the polymer active layer through encapsulation.[19,21] The operational stability of PTFTs continues to improve, but more improvements should be made. Semiconducting and insulating polymer blends or copolymers have attracted considerable research interest.[19,21−27] In general, the presence of an insulating component tends to degrade electrical characteristics by diluting the current density of the active layer.[22−24] However, several reports showed that semiconducting/insulating polyblends can improve or maintain the electrical characteristics of PTFTs. For example, Arias et al.[21] developed semiconducting poly[5,50-bis(3-dodecyl-2-thienyl)-2,20-bithiophene] (PQT-12)/insulating poly(methyl methacrylate) (PMMA) polyblend-based PTFTs with improved environmental stability. In these transistors, PMMA is self-encapsulated on top of the blends upon an octyltrichlorosilane-treated silicon dioxide (SiO_2) dielectric by vertical phase separation. Qiu et al.[26] reported poly(3-hexylthiophene) (P3HT; semiconducting component):-polystyrene (PS; insulating component) polyblend-based PTFTs with high performance. This high performance is attributed to the formation of interconnected P3HT nanowires embedded in a PS matrix by controlling solvent-assisted solidification. Kergoat et al.[27] presented P3HT/PMMA polyblend-based PTFTs with slightly improved I_{off} levels. The mobility of these P3HT/PMMA polyblend-based PTFTs is comparable with that of pure P3HT because of the lateral phase

DOI: 10.1021/acsami.5b03864
ACS Appl. Mater. Interfaces 2015, 7, 16486−16494

separation of the binary blends. Wu et al.[19] reported an enhanced electrical performance of PTFTs by preparing a semi-interpenetrating semiconducting P3HT/insulating PMMA active layer with an interdiffused interface. Semiconducting/insulating blends offer a simple but useful method for controlling device characteristics by developing an active channel with various microstructures.

In this study, we demonstrate that fast-switching PTFTs with an uncommon nondecaying feature (even over a long-term dynamic continuous operation with high gate bias) can be obtained by using semiconducting/insulating polyblends as the active layer with multiple-scale phase-separated (MSPS) morphology. Different from previously discussed polyblend-based PTFTs, the MSPS morphology is a distinct type of polymeric active layer.[21−27] This study is the first to observe the current growth and absence of decay in PTFTs, even under continuous DC gate voltage sweep. Furthermore, the PTFTs in this study exhibit several advanced electrical characteristics, such as fast switching, cutoff leakage pathway, and excellent gas sensing. The interfacial and phase-separated microstructure of the blending active layer and its effect on the electrical performance of PTFTs are comprehensively investigated by impedance admittance and polarization-electric field ($P-E$) analyses, grazing incident X-ray diffraction (GIXD), atomic force microscopy (AFM), electrostatic force microscopy (EFM), transmission electron microscopy (TEM), and AFM-Raman microspectroscopy. Finally, studies of the polyblends with MSPS morphology allow us to propose a concept of the active layer for an ideal-like PTFT.

2. EXPERIMENTAL SECTION

P3HT (M_w of 87000 g/mol, 98.5% regioregular) and PMMA (M_w of 35000 g/mol) were purchased from Aldrich Chemical Co. and used without further purification. The 0.34 wt % P3HT solution in *p*-xylene was prepared first. Then, PMMA was added to the P3HT solution at various compositions to form different blending solutions. Before deposition of the polymer active layer, the TFT substrate was treated with oxygen plasma (Drytek MS6 Plasma Etcher Mega Strip 6). The polymer active layer was spin-coated from these polymer solutions on the TFT substrate and baked at 120 °C for 2 h. The thicknesses of the polymer films were determined by an Alpha-step (Tencor Instruments, Alpha-step IQ) and AFM (XE-100, Park Systems). The water contact angle was analyzed using the OCA15 contact angle goniometer (Dataphysics Co.). The polarization density and dielectric constant characterization of the metal/gate insulator/semiconductor/metal (MISM) and MIM diodes were evaluated using an Agilent E4980 LCR meter. The PTFTs were characterized using a Keithley 4200-SCS. The GIXD of polymer samples were performed at the BL01C2 beamline of the NSRRC; a detailed description of the experimental procedure can be found in the Supporting Information. The EFM measurements were performed by commercial AFM (XE-100, Park Systems). Laser-excited Raman images were acquired at 633 and 488 nm from a RAMaker system mounted with one Nanonics MV4000 nanostage and one Andor Newton TE-cooled CCD of 2048 × 512 pixels as integrated by Protrustech Corporation Limited. TEM observations were made through the use of a JEOL JEM-1400 instrument operated at 120 kV, and bright-field images were obtained using a Gatan digital detector. Quantum chemical calculations: The geometry of the monomer of PMMA was optimized at the density functional theory (DFT) level by using the B3LYP functions with the 6-31G(d) basis set, and the molecular dipole moment was evaluated. All of the calculations were performed using the Gaussian suite of programs.

3. RESULTS AND DISCUSSION

3.1. Electrical Characteristics of PTFTs. This study employed the standard inverted-coplanar TFT structure with SiO_2 as the gate insulator, indium tin oxide (ITO) as the gate, source, and drain electrodes (Figure 1a) as described elsewhere,[12] and called it a TFT substrate. Such TFT substrates are durable[12] and allow investigation of the effects of the polyblend structure on the electrical characteristics of the PTFT. P3HT/PMMA-blend solutions with different P3HT and PMMA weight ratios were prepared by adding PMMA at various compositions to the P3HT *p*-xylene solution. All films were prepared from the resulting polyblend solutions on the TFT substrate.

Panels b and c in Figure 1 show a comparison of the typical transfer and output characteristics of the P3HT-based TFTs with and without PMMA blending, respectively. In particular, we focus on two significant TFT parameters, namely, S characteristics and I_{off} level, which are hard to change by varying TFT structural configurations. The S characteristic reflects the quality of the active channel. A low I_{off} and steep S standing are particularly important in real applications and in determining the speed and power of a device. By contrast, μ_{FE} is highly dependent on channel dimensions and other parameters (e.g., capacitance and overestimated μ_{FE} are observed using high-frequency capacitance and a theoretical dielectric constant). High bulk conductance also leads to an overestimated μ_{FE}. Also, the use of a standard MOSFET equation to extract the μ_{FE} can give significantly overestimated results.[28] Therefore, our focus in this paper is to discuss the factors affecting S and I_{off} and operational stability of PTFTs instead of μ_{FE}.

The pristine P3HT-based TFTs displayed poor S behavior (~17.0 ± 3.0 V/dec) and a relatively high I_{off} level of >10^{-9} A. The inferior field-effect characteristics in PTFTs are quite common given the easy doping nature of conjugated polymers. The unintentional doping of the polymer film benefits the film's conductivity even with off-state PTFTs; thus, the I_{off} values of most PTFTs reported in the literature are usually higher than 10^{-7} to 10^{-9} A.[11,13,17] This doping also weakens the gate-to-channel controllability.[13,19] After blending P3HT with PMMA, the S and I_{off} levels significantly improved with an absence of hysteresis behavior. The P3HT/PMMA (25:75) devices exhibit an optimal S value of <1.0 V/dec, which is an outstanding value compared to that of most PTFTs reported in the literature. Meanwhile, the maximum I_D was also enhanced by the blending of the insulating component, which corresponds to a significant improvement in μ_{FE}, especially at small operating voltages (Figure S1, Supporting Information). In the linear regime, I_{DS} was enhanced 3× compared to that of pure P3HT-based PTFTs, which corresponds to an increase of at least ~3× of μ_{FE}.

Early studies have found that the measured mobilities of organic/polymeric TFTs strongly increase with increasing conductivity of the active layers; thus, large on/off ratios and high mobilities are not to be expected simultaneously.[29,30] That means it is difficult to improve the S and I_{off} level while increasing μ_{FE} of PTFTs. Therefore, it is quite reasonable that the observed μ_{FE} in this study is not particularly high (~10^{-2} cm^2 V^{-1} s^{-1}) compared to that of previous studies performed by other researchers.[11] Evidently, an appropriate amount of PMMA could actually boost the gate-to-channel control of devices. More particularly, throughout the continuous dynamic operation of the P3HT/PMMA (25:75) devices, the output

DOI: 10.1021/acsami.5b03864
ACS Appl. Mater. Interfaces 2015, 7, 16486−16494

current (I_D) increased and was stable even with a relatively large gate bias (Figure 1d). The current behavior cannot be caused by the gate current (I_G, see right axis of Figure 1d). By contrast, I_D decays rapidly over time for pristine P3HT PTFTs, and the decay behavior is common in organic and polymeric TFTs.[6,9,12] However, P3HT-based PTFTs can still exhibit almost unchanged μ_{FE} with prolonged operation as long as the recovery or static stability is adequate.[6−8,12,21,24] However, in real applications, the most serious problem of PTFTs is the significant decay (I_D) associated with an unstable threshold voltage (V_{th}) under continuous dynamic operations. This problem is otherwise known as dynamic instability and is still unresolved. Here, we show that PTFTs with adequate dynamic stability are possible.

Given the wide variety of microstructures of polyblends, which highly depend on fabrication conditions (e.g., solvent and solvent composition, concentration, molecular weight, temperature, processing method, and so on), the completely different results from previous studies is unsurprising.[21,22,27] Therefore, this study aims to explore outstanding stable and switch electrical properties on the basis of present blending films instead of through the optimization of fabrication processes. Moreover, when the PMMA fraction was lower than 50 wt %, no significant improvements in electrical characteristics were observed in PTFTs, and the corresponding polymeric active layers also show small differences in their microstructure. In the following section, we will focus on analysis of the samples with significant differences.

3.2. Interface Properties and Charge Trap Analysis.

The interfacial properties of the active layer and gate dielectric have critical roles in determining the electrical characteristics of TFTs because the charge transport occurs on a thin layer near the dielectric interface. The S is an indicator of the density of traps (D_t) in the channel, including the deep bulk traps (D_b) and interface traps (D_{it}), given by the formula[30]

$$S = \frac{kT\ln 10}{e}\left(1 + \frac{e}{C_i}D_t\right) = \frac{kT\ln 10}{e}\left[1 + \frac{e}{C_i}(\sqrt{\epsilon_s D_b} + eD_{it})\right] \quad (1)$$

where k is Boltzmann's constant, T is temperature, e is electron charge, C_i is gate capacitance, and ϵ_s is the dielectric constant of the semiconductor. Thus, a low S value reflects a low trap density. For a pristine P3HT channel, the observed D_t was 2.22 × 10^{13} 1/eV·cm^2. The best results were obtained using the P3HT/PMMA (25:75) active layer with a D_t of only 1.13 × 10^{12} 1/eV·cm^2. The effect of the charge trap on the blending systems significantly decreased. After adding 25, 50, and 90 wt % of PMMA, there was only slight improvement in the D_t of 1.30 × 10^{13}, 1.60 × 10^{13}, and 1.72 × 10^{13} 1/eV·cm^2, respectively.

Impedance-admittance analyses of an MISM diode configuration[31,32] were also performed to extract the D_{it} and mean interface trap time constant (τ_{it}) of the interface of the active layer and gate insulator, as shown in Figure 2a. The frequency-dependent conductance at a given V_G was measured. The single time constant model was used, and the equivalent parallel conductance (G_p) is given by[31]

$$\frac{G_p}{\omega} = \frac{q\omega\tau_{it}D_{it}}{1 + (\omega\tau_{it})^2} \quad (2)$$

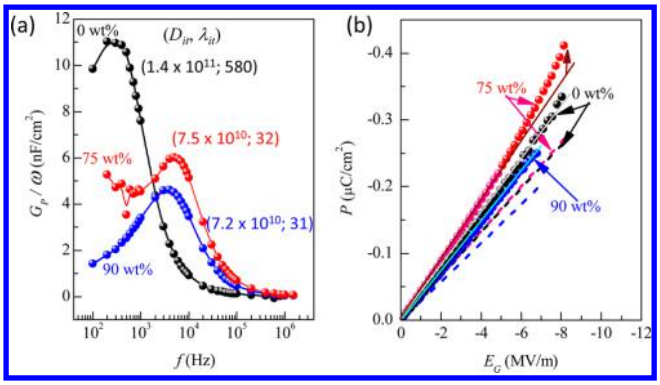

Figure 2. (a) Frequency-dependent conductance (G_p/ω) characteristics and (b) polarization (P) versus applied gate electric fields (E_G) at 300 Hz of the MISM diodes with the P3HT:PMMA blending films having different weight percents of PMMA. In (a), the extracted interfacial trap density (D_{it}, unit: 1/eV·cm^2) and mean interface trap time constant (τ_{it}, unit: μs) are also indicated. In (b), the dashed line was obtained at high frequency (1 MHz), which corresponds to the absence of the dipole effect. The solid line serves as a guideline.

where ω is the angular frequency, and q is the charge of the electron. The maximum value of G_p/ω occurs at $\omega\tau_{it} = 1$. The extracted D_{it} of the pure P3HT devices (1.4 × 10^{11} eV^{-1} cm^{-2}) is 1.87 and 1.94 times larger than that of the P3HT/PMMA (25:75, 7.5 × 10^{10} eV^{-1} cm^{-2}) and P3HT/PMMA (10:90, 7.2 × 10^{10} eV^{-1} cm^{-2}) devices, respectively. The corresponding τ_{it} value (>500 μs) is much larger than that of the blending devices (only ∼30 μs). Several previous studies have emphasized that the PMMA modification of the dielectric gate surface is useful in reducing surface traps.[32−34] Thus, several PMMA chains have been deduced to diffuse to the bottom of the active channel and hence PMMA-rich thin layer, thereby modifying the SiO_2 surface. With increased PMMA content, this finding becomes more significant as D_{it} decreases. Moreover, the significantly shortened τ_{it}, which reflects the trapping−detrapping rate, supports a stable I_D in continuous operations through dynamic programming. Interestingly, the 90 wt % PMMA sample exhibited the better D_{it} and τ_{it} values than those of the 75 wt % PMMA sample. This result does not explain the electrical properties of the corresponding PTFTs, and theoretically, the best result should be exhibited by the 75 wt % PMMA sample instead of the 90 wt % PMMA sample. This result may be caused by the excessive amount of PMMA in the channel. This excessive PMMA may have interrupted the conducting channel of P3HT and substantially increased the structural defects as bulk charge traps.

The molecular dipoles in the PMMA buffer layer (note: the main dipole is the O = C-OCH_3 group, which has a dipole moment of −1.8 D) can be aligned by a high gate electric field (E_G) and thus generate a useful dipole field (E_d) to enrich the charge accumulation in the channel and enhance the electrical performance of the organic TFTs.[34] The P−E analysis of the MISM diodes (Figure 2b) also provided evidence for the enhanced polarization, such as the charge accumulation caused by the PMMA modification on the P3HT/PMMA (25:75) device. The increased slope of the P−E curve with high E_G demonstrates that a high field is necessary to align these randomly incorporated dipoles of the amorphous PMMA to obtain a useful E_d. This observation is in agreement with the previous finding on the pentacene-based TFTs with a PMMA buffer layer.[34] The current growth phenomenon of the

DOI: 10.1021/acsami.5b03864
ACS Appl. Mater. Interfaces 2015, 7, 16486−16494

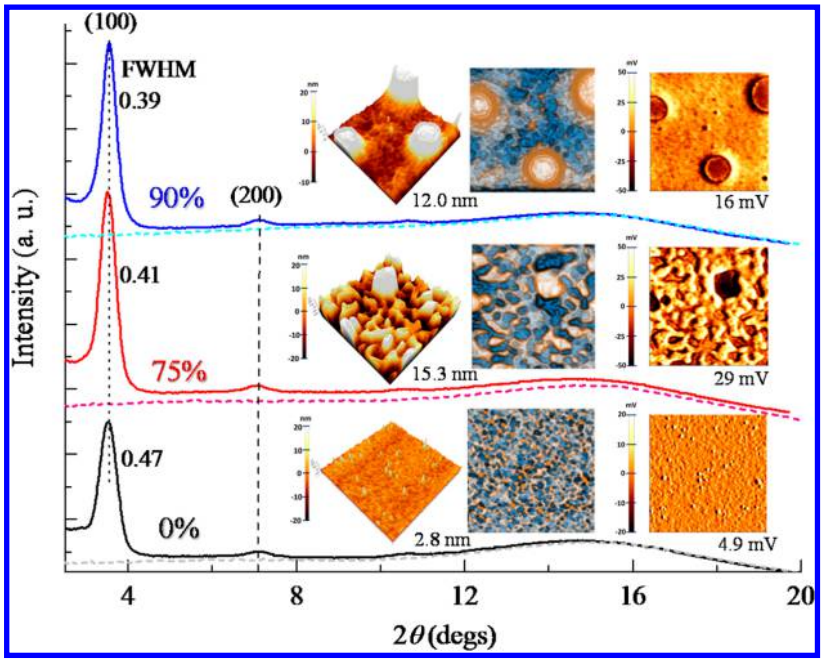

Figure 3. Out-of-plane (solid lines) and in-plane (dashed lines) GIXD spectra of the P3HT:PMMA blending films with different weight percents of PMMA. The fwhm of the (100) peak is also shown. Insets: the corresponding AFM topography (left panels) and phase (middle panels) images and EFM images (right panels). The values of root-mean-square roughness were also indicated on the bottom right corner.

corresponding PTFTs at the early continuous operations (before ~200 s, Figure 1d) can be explained by the time required to align the PMMA dipoles with the E_G to generate a useful E_d to aid in the charge accumulation. That means that E_d increased with increased time and was then saturated for a certain period of time. Furthermore, the increased amount of charge was caused by E_d, which was required to overcome the negative effects (such as charge trap and bias stress effects) present during long-term continuous operations of PTFTs. However, for the P3HT/PMMA (10:90) device, a small dipole effect, probably because of the excessive amount of PMMA that diffuses to the bottom of the active channel, and a significant increase in the film thickness were observed. Such a situation thus requires a higher E_G to obtain a useful E_d. In the following section, details on the microstructural studies of the corresponding active layer are provided to obtain deeper insights into the origins of the excellent electrical properties of the blending film-based PTFTs.

3.3. Microstructural and Morphological Analysis. The GIXD was first measured in both in-plane and out-of-plane setup to evaluate the distribution of growth orientation of P3HT crystalline domains (Figure 3) because charge transport within the blend film can only occur in a semiconducting component. The results reveal that the edge-on organization of P3HT molecular segments[35] was dominant and remained unchanged despite PMMA blending. Interestingly, the addition of considerable amounts of insulating PMMA (up to nine times that of P3HT) did not reduce the size of the P3HT crystalline domains along the *a*-axis (L_a) according to the half-width of the (100) diffraction peak. We noted that the thicknesses of the blending films (e.g., 168.8 ± 9.91 nm and 181.3 ± 9.32 nm of the P3HT:PMMA (25:75) and (10:90) films, respectively) are higher than that of the pure P3HT film (102.5 ± 8.09 nm), which may thus allow for the increase in L_a. However, absorption spectra (Figure S2, Supporting Information) indicate that the resultant blend films were considerably more amorphous than the pristine P3HT films.

The phase distribution within the blending film was further explored by obtaining AFM and EFM images. The topographic image of the blending films (inset of Figure 3) given by AFM reveals granular domains with diameters varying from 300 nm to >1 μm. The granular domains are surrounded by network regions of the P3HT/PMMA mixture as an approached status of phase separation. Water contact angle (θ) measurements of the films were also performed. The pure P3HT film shows the θ value of 106.1 ± 0.25°, indicating a hydrophobic feature. With an increasing amount of PMMA in the blend films, the θ values decreased to 101.8 ± 1.64° and 92.2 ± 1.41° of the P3HT/PMMA (25:75) and (10:90) films, respectively. This indicated an increased amount of PMMA on the surface of the blending films. To classify the domains/areas of PMMA and P3HT, we further explored the EFM results (inset of Figure 3, right panels). For the pure P3HT film, the distribution of surface potential was homogeneous with a root-mean-square (RMS) value of only 4.8 mV. Differing for the blending films, the distribution of surface potential varied with larger fluctuations. For the P3HT/PMMA (25:75) film, the RMS surface potential increased to 29.2 mV, which is twice that of the P3HT/PMMA (10:90) film (15.6 mV). It is thus realized that these granular domains with relatively low potential (i.e., the dark area of the EFM image) should be classified as local PMMA-rich domains. By contrast, brighter regions observed on obtained EFM images are related to higher surface potential and therefore include the organization of semiconducting P3HT. Considering both the AFM and EFM images of the P3HT/PMMA (25:75) films, the sizes of local PMMA-rich granular domains are mostly <0.5 μm, and only few of them are close to 1 μm. In between these scattered PMMA-rich granular domains, the surrounding network regions consist of a mixture of PMMA and P3HT molecular chains continuously through

DOI: 10.1021/acsami.5b03864
ACS Appl. Mater. Interfaces 2015, 7, 16486−16494

the blended film. This phase morphology is considered to be present at the early stage of phase separation.

For crystallization within the pure P3HT thin film, based on the obtained AFM and EFM results, small P3HT crystallites (tiny bright domains in AFM images) were developed and scattered within the thin film upon solvent evaporation. This dense distribution of small crystallites is a consequence of random nucleation within the thin film, resulting in large interfacial areas. These randomly nucleated crystallites of P3HT (blue domains in AFM images) are separated by amorphous grain boundaries (orange domains). Thus, as it involves efficient nucleation, charge carriers are easily trapped before jumping to neighboring crystalline domains. By contrast, within the P3HT/PMMA (25:75) films, according to the measured RMS surface potential shown in Figure 3, P3HT crystalline phases (blue regions) were preferably developed within network regions. Furthermore, upon closely examining the TEM image shown in Figure 4, several fringes of P3HT

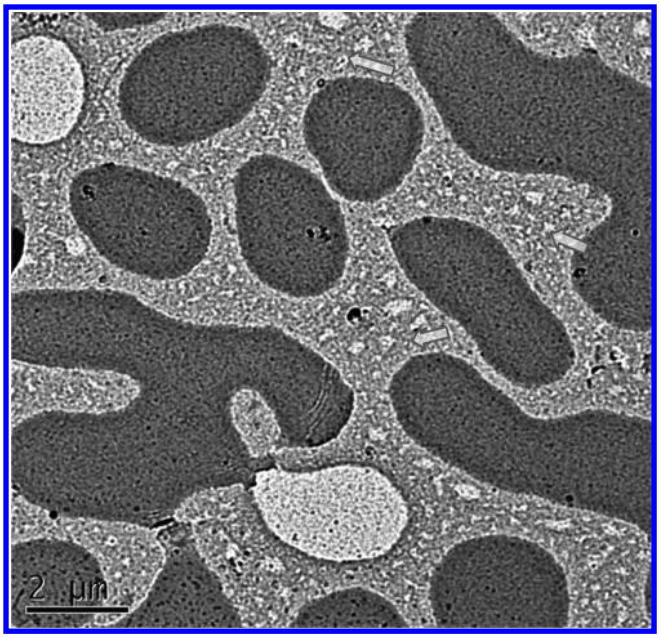

Figure 4. Electronic micrograph of phase-separation morphology within the P3HT/PMMA (25:75) film. The darker granular domains are the PMMA-rich regions, and the spread of the P3HT/PMMA mixture results in surrounding network morphology. Some fringes of P3HT crystalline lamellae within the network region are indicated by arrows.

crystalline lamellae can be identified (indicated by arrows). According to these experimental observations, the distribution of amorphous PMMA domains within the thin film is capable of confining the crystallization of P3HT but is not, however, able to guide the crystallization orientation. Thus, the crystal orientation of P3HT within a P3HT/PMMA thin film remains random with edge-on azimuthal orientation. Furthermore, only scattered PMMA-rich granular domains were observed, and P3HT-rich domains are not discernible. It is derived that the quick crystallization of P3HT will freeze following phase separation and prevent the formation of a P3HT-rich domain. Hence, this observed morphology can be considered as a frozen state of phase separation by the crystallization of P3HT.

According to these results, the crystallization of the P3HT component is realized to be more or less confined within thinner network regions because scattered PMMA-rich granular domains are less favored for the propagation of crystallization. Furthermore, the nucleation efficiency of P3HT within thinner network regions can be largely reduced by the diluent effect of PMMA, which allows each crystalline domain to propagate continuously without being arrested by neighboring crystallization events. Hence, the $\pi-\pi$ stacking of the P3HT conjugated backbones can be continuously established within network regions, which helps the charge transportation through the thin film without being interrupted by domain boundaries. This identification of phase separation and the following confined crystal growth of P3HT thus provides the foundation for achieving a constant drain current I_D over time.

Although the involved phase separation via blending the amorphous PMMA component reduces the crystallinity and number of nuclei, the available propagation of crystal growth within the confined network regions helps to reduce the areas of domain boundaries and thus results in uninterrupted charge transportation. Nevertheless, when a great excess of PMMA content is included, as observed in the P3HT/PMMA (10:90) film, P3HT chains are seriously diluted and loosely dispersed within the thin film. As a result, the efficiency of molecular supply turned out to be a detrimental issue for the continuous growth of crystalline domains, and scattered crystalline domains separated with amorphous domains consequently developed. Thus, it is realized that the amount of PMMA within a polymeric active layer should be adjusted for continuous propagation of P3HT crystalline domains. Including an excess amount of PMMA results in a scattered distribution of small crystalline domains and creates lots of domain boundaries that are detrimental to charge transportation. The microstructural analysis provides a reasonable basis for interpreting the D_b and D_{it} results of different blending films due to structural defects.

3.4. AFM-Raman Mapping Analysis of the Intrachain Order of the P3HT Chains. Integrated AFM-Raman mapping analysis is relevant to further understanding the relationship between the microstructure of P3HT chains and the TFT characteristics. The intrachain order of conjugated polymer chains (i.e., in terms of the effective conjugated length (L_c)) has been proven to exert considerable effects on the electrical characteristics of TFTs.[12,36,37] Raman spectroscopy is a powerful analytical tool for studying the L_c of P3HT chains by detecting the strongest symmetric C_α-C_β stretching deformation of the thiophene ring at approximately 1440 cm^{-1} to 1460 cm^{-1}, denoted as the ν_s band.[12] The peak center of the band is an index of L_c (i.e., increasing the L_c causes the band to downshift). Different excitation lines were used to extract the L_c information on P3HT chains within the films. The energy of the 633 nm laser was located at the red edge of the P3HT absorption (Figure S2, Supporting Information); therefore, any enhancement of this featured Raman band is related to the highly ordered crystalline structure of P3HT with longer L_c.[12] By contrast, the distribution of P3HT chains in amorphous regions with a short L_c can be observed at an excitation wavelength of 488 nm (Figure S2, Supporting Information).[12,38] Accordingly, the peak maximum of the ν_s band shifts from 1443 cm^{-1} at 633 nm excitation to 1453 cm^{-1} at 488 nm excitation. The corresponding Raman intensity maps of the ν_s band are shown in Figure 5. The images of pure P3HT films show a homogeneous distribution of the bands at both 633 and 488 nm excitations, which indicate the scattering of small amorphous and crystalline regions within the thin film. No particularly large crystalline or amorphous domains were

DOI: 10.1021/acsami.5b03864
ACS Appl. Mater. Interfaces 2015, 7, 16486−16494

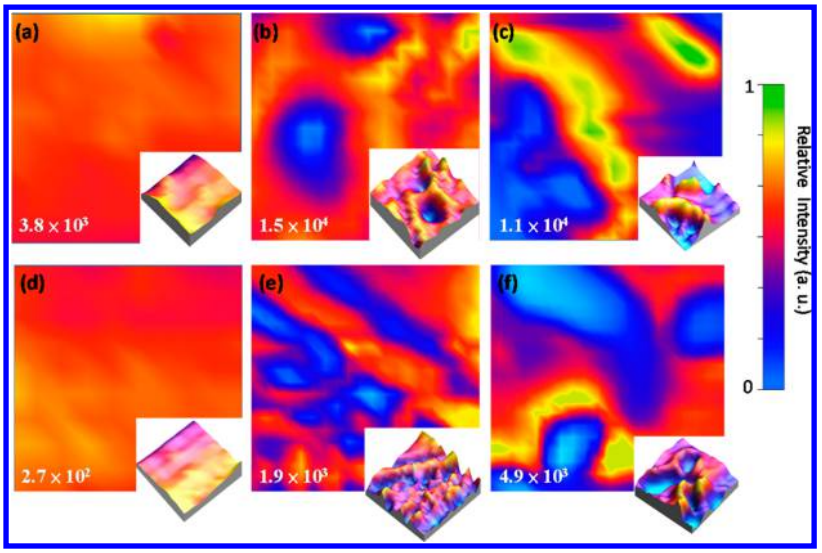

Figure 5. Raman intensity images (15 × 15 μm^2) of the pristine P3HT (a and d), 25:75 P3HT/PMMA (b and e), and 10:90 P3HT/PMMA (c and f) thin films. (a–c) λ_{exc} = 633 nm, the relative intensity of the peak at 1443 cm^{-1}. (d–f) λ_{exc} = 488 nm, the relative intensity of the peak at 1453 cm^{-1}. Images at the bottom right corner: corresponding 3D images (20 × 20 μm^2). The values of root-mean-square roughness are also indicated in the bottom left corner.

formed. This phenomenon is common in single-component polymer films. However, very different Raman images of blending films were observed as compared that of the pure P3HT film. Within the blending films, the PMMA-rich domains (blue areas) can be clearly seen. Notably, some areas around the PMMA-rich domains exhibit relatively strong ν_s bands (inset of Figure 5b), which indicates the organization of well-extended P3HT chains confined around interfaces. Such phenomena are increasingly pronounced in the P3HT/PMMA (10:90) sample.

Figure 5e shows some small local P3HT-rich areas in which short L_c chains were formed in the P3HT/PMMA (25:75) film. Comparison of the two maps in Figure 3b and e shows that the fraction of the crystalline area (f_c) is larger than that of the amorphous area (f_a). More importantly, crystalline P3HT chains with long L_c exhibit interconnections that are superior to those of the amorphous portions. By contrast, for the P3HT/PMMA (10:90) film, the f_a in Figure 5c is larger than the f_c in Figure 5f. Compared with the crystalline P3HT regions with poor interconnections (Figure 5c), the amorphous regions that consist of short L_c chains still have some interconnections.

These observations provide useful information in interpreting the electrical performance of the blending films. Compared to the pure P3HT film, the P3HT/PMMA (25:75) film has continuous interconnected regions of long L_c P3HT portions, which apparently provide an efficient pathway for charge transport within the active layer of PTFTs. However, for the P3HT/PMMA (10:90) film, the spread of an excess amount of PMMA is able to interrupt the interconnection of the long L_c P3HT portions, thereby leading to significant reduction in I_{DS}. Meanwhile, the leakage pathway was also suppressed. Kergoat et al. have found that the formation of insulating domains decreases the leakage current of PTFTs.[27] We have also found that doping the PMMA into P3HT:phenyl-C61-butyric acid methyl ester blending films, which serve as the active layer for solar cells, can also lessen the leakage pathways.[39] Alternatively, the unintentionally introduced impurities can also be absorbed by the PMMA domains because of a high free volume caused by the amorphous nature and electron-donating character of the ester groups. Moreover, amorphous PMMA regions are easily swollen by absorbing a small amount of water,[40] which in turn reduces the moisture effects on the electrical properties of the blending film-based PTFTs and results in a very low I_{off} level. These observations provide a reasonable background for developing highly stable PTFTs able to yield initial current growth and finally reach stable saturation behavior. Following this concept, we further found that the P3HT/PMMA (25:75)-based TFTs exhibiting excellent gas sensing sensitivity because of the presence of PMMA domains in the active channel of PTFTs could be viewed as a gas highway (Figure S3, Supporting Information, detailed studies on this subject will be published elsewhere).

3.5. Active Layer Structure for Ideal-Like Field-Effect-Modulated PTFTs. On the basis of the observations described above, the microstructure of the P3HT:PMMA (25:75) blending film can be viewed as an idealized active layer for ideal-like PTFTs (Figure 6). The proposed MSPS morphology of the blending film is a unique phase-separated structure and is not a purely lateral nor vertical phase-separated structure. Such an MSPS morphology was not observed by Kergoat et al.,[27] who studied a binary blend between P3HT and PMMA with different microstructures by lateral phase separation. They observed that P3HT domains change into isolated islands when the PMMA content is over 70%, thus lowering the electrical performance of the corresponding PTFTs. This difference may be ascribed to different fabrication conditions (in their case, different molecular weights of P3HT and PMMA were used, and the films were deposited from different solvents). A well-defined continuous semiconducting crystalline phase with minimized domain boundaries can be established under the confinement effect of incompatible insulating components, thus reducing the bulk traps from structural defects for efficient electrical switching and charge transportation. Introducing the PMMA into the P3HT films can cause the P3HT chain conformations to become more homogeneous and can suppress the formation of vacancies and leakage pathways. As discussed earlier, a basic requirement for gate dielectric is to provide a clean interface with a semiconductor (i.e., one with

DOI: 10.1021/acsami.5b03864
ACS Appl. Mater. Interfaces 2015, 7, 16486–16494

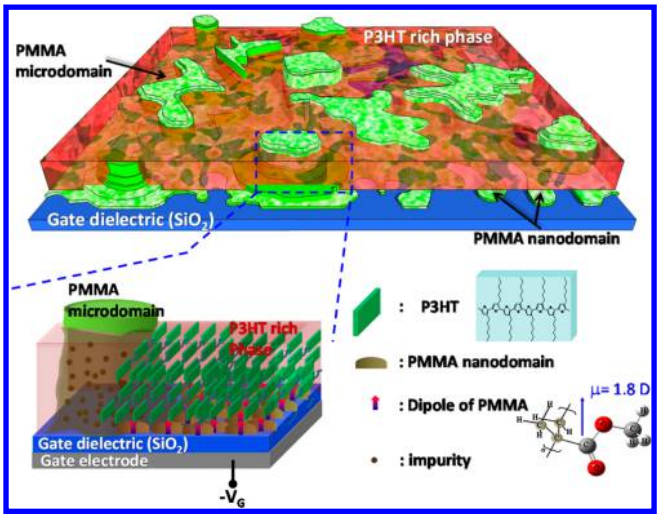

Figure 6. Schematic diagram of the blending film with multiscale phase-separated morphology. During turn-on of PTFTs, the molecular dipole of the PMMA nanodomain can be aligned with the use of applied external gate voltage (V_G) to aid in charge accumulation at a relatively small given voltage. The diagram also shows that unintentional impurities can be absorbed by the PMMA domains. The calculated dipole moment (μ) based on a monomer of PMMA is also shown by density functional theory (DFT) with B3LYP/6-31G method, and the vector indicates the direction of the dipole moment.

minimized interfacial traps). Moreover, to ensure fast charge accumulation at a relatively low given voltage, the gate dielectric with built-in internal electric field is addressed. In practice, the spontaneous MSPS process of the P3HT:PMMA polyblends provides a simple method to achieve such goals, that is, the PMMA thin layer at the seminconductor/gate dielectric interface can provide the above functions. In this case, PMMA formed a valley topograph on the bottom of the blend. This finding also differs from the results of Arias et al.,[21] who observed the PMMA on top of the PQT-12/PMMA blends. Finally, the effects of unintenational impurities on the electrical switch characteristics of PTFTs should be eliminated. Built-in amorphous PMMA-rich multiple scale domains of the blending films serve as an internal adsorbent for such impurities. Thus, ideal-like PTFTs with high dynamic operational stability can be achieved. Even in ambient air, the PTFTs still work well and can serve as a good gas sensor. Additionally, various fabrication conditions of the blending films were also tested, such as different compositions of the blending films, solvent used, molecular weight of PMMA, and so forth. Among them, we highlighted that the present P3HT:PMMA (25:75) blending film-based PTFTs still exhibit the best results, which can be easily reproduced.

4. CONCLUSION

Introducing an appropriate amount of insulating PMMA into the semiconductive P3HT active channel forms ideal-like PTFTs because of the well-defined phase-separated structure of the binary blends. Given its MSPS morphology, the P3HT/PMMA (25:75) PTFTs exhibit a unique nondecaying feature. Although significant progress has been made in enhancing the static stability of polymeric TFTs in recent years, to the best of our knowledge, such dynamic operational stability phenomena, which are extremely important in real applications, have not yet been observed in PTFTs. Combined with charge trapping and microstructural analyses, the excellent PTFT characteristics of P3HT/PMMA (25:75) devices can be attributed to the promising propagation of the crystalline region within blending films via the aid of the diluent effect of the insulating PMMA component. The subsequent formation of the P3HT crystalline network results in the formation of continuously interconnected active channels for high-speed charge transportation without being interrupted by domain boundaries. The distribution of PMMA components also helps to modify the SiO_2 surface, thereby yielding excellent gate modulation for the conductance channel. Such features can be further strengthened by the moisture and impurity absorption functions of the PMMA-rich multiple scale domains. The presence of PMMA-rich domains within the active channel also creates a gas highway for PTFTs with excellent gas sensing functions, an additional benefit in practical applications. Finally, the requirements of achieving an ideal-like polymer-based active channel for TFTs were proposed. Although the mobility is not particularly high, the unique electric properties of the blending films have a wide range of potential applications, such as in TFT devices, switching devices, inverter and integrated circuits, and sensor devices.

■ ASSOCIATED CONTENT

Supporting Information

Electrical characteristics of PTFTs, absorption spectra and theoretical fitting procedures, experimental details of GIXD, Raman spectroscopy study of the effective conjugation length of P3HT, and P3HT/PMMA-based PTFT as a gas sensor. The Supporting Information is available free of charge on the ACS Publications website at DOI: 10.1021/acsami.5b03864.

■ AUTHOR INFORMATION

Corresponding Authors

*E-mail: shlcheng@mail.ncku.edu.tw.
*E-mail: jrjeng@mail.ncku.edu.tw.

Notes

The authors declare no competing financial interest.

■ ACKNOWLEDGMENTS

This work was supported by the Ministry of Science and Technology, Taiwan, through Grants NSC101-2221-E-006-163-MY3 and NSC102-2221-E-006-220-MY3. The authors acknowledge the technical support of the imaging system for vibrational spectroscopy provided by the Instrument Center of National Chung Hsing University. We are grateful to the National Center for High-performance computing of Taiwan for computer time and facilities.

■ REFERENCES

(1) Skotheim, A., Reynolds, J. R., Eds. *Handbook of Conducting Polymers*, 3rd ed.; CRC press: Boca Raton, FL, 2007.
(2) Sekitani, T.; Someya, T. Stretchable, Large-Area Organic Electronics. *Adv. Mater.* **2010**, *22*, 2228−2246.
(3) Schwartz, G.; Tee, B. C.-K.; Mei, J.; Appleton, A. L.; Kim, D. H.; Wang, H.; Bao, Z. Flexible Polymer Transistors with High Pressure Sensitivity for Application in Electronic Skin and Health Monitoring. *Nat. Commun.* **2013**, *4*, 1859.
(4) Salleo, A.; Kline, R. J.; DeLongchamp, D. M.; Chabinyc, M. L. Microstructural Characterization and Charge Transport in Thin Films of Conjugated Polymers. *Adv. Mater.* **2010**, *22*, 3812−3838.
(5) Noriega, R.; Rivnay, J.; Vandewal, K.; Koch, F. P. V.; Stingelin, N.; Smith, P.; Toney, M. F.; Salleo, A. A General Relationship Between Disorder, Aggregation and Charge Transport in Conjugated Polymers. *Nat. Mater.* **2013**, *12*, 1038−1044.

DOI: 10.1021/acsami.5b03864
ACS Appl. Mater. Interfaces 2015, 7, 16486−16494

(6) Mathijssen, S. G. J.; Cölle, M.; Gomes, H.; Smits, E. C. P.; De Boer, B.; McCulloch, I.; Bobbert, P. A.; De Leeuw, D. M. Dynamics of Threshold Voltage Shifts in Organic and Amorphous Silicon Field-Effect Transistors. *Adv. Mater.* **2007**, *19*, 2785−2789.
(7) Ficker, J.; Ullmann, A.; Fix, W.; Rost, H.; Clemens, W. Stability of Polythiophene-Based Transistors and Circuits. *J. Appl. Phys.* **2003**, *94*, 2638−2641.
(8) Salleo, A.; Endicott, F.; Street, R. A. Reversible and Irreversible Trapping at Room Temperature in Poly(thiophene) Thin-Film Transistors. *Appl. Phys. Lett.* **2005**, *86*, 263505.
(9) Street, R. A.; Endicott, M. L.; Ong, B. Extended Time Bias Stress Effects in Polymer Transistors. *J. Appl. Phys.* **2006**, *100*, 114518.
(10) Umeda, T.; Tokito, S.; Kumaki, D. High-Mobility and Air-Stable Organic Thin-Film Transistors with Highly Ordered Semiconducting Polymer Films. *J. Appl. Phys.* **2007**, *101*, 054517.
(11) Sirringhaus, H. Reliability of Organic Field-Effect Transistors. *Adv. Mater.* **2009**, *21*, 3859−3873.
(12) Cheng, H. L.; Lin, J. W.; Jang, M. F.; Wu, F. C.; Chou, W. Y.; Chang, M. H.; Chao, C. H. Long-Term Operations of Polymeric Thin-Film Transistors: Electric-Field-Induced Intrachain Order and Charge Transport Enhancements of Conjugated Poly(3-hexylthiophene). *Macromolecules* **2009**, *42*, 8251−8259.
(13) Cheng, H. L.; Lin, W. Q.; Wu, F. C. Effects of Solvents and Vacancies on the Electrical Hysteresis Characteristics in Regioregular Poly(3-hexylthiophene) Organic Thin-Film Transistors. *Appl. Phys. Lett.* **2009**, *94*, 223302.
(14) Bronstein, H.; Chen, Z. Y.; Ashraf, R. S.; Zhang, W. M.; Du, J. P.; Durrant, J. R.; Tuladhar, P. S.; Song, K.; Watkins, S. E.; Geerts, Y.; Wienk, M. M.; Janssen, R. A. J.; Anthopoulos, T.; Sirringhaus, H.; Heeney, M.; McCulloch, I. Thieno[3,2-*b*]thiophene-Diketopyrrolopyrrole-Containing Polymers for High-Performance Organic Field-Effect Transistors and Organic Photovoltaic Devices. *J. Am. Chem. Soc.* **2011**, *133*, 3272−3275.
(15) Tsao, H. N.; Cho, D. M.; Park, I.; Hansen, M. R.; Mavrinskiy, A.; Yoon, D. Y.; Graf, R.; Pisula, W.; Spiess, H. W.; Müllen, K. Ultrahigh Mobility in Polymer Field-Effect Transistors by Design. *J. Am. Chem. Soc.* **2011**, *133*, 2605−2612.
(16) Chen, H.; Guo, Y.; Yu, G.; Zhao, Y.; Zhang, J.; Gao, D.; Liu, H.; Liu, Y. Highly π-Extended Copolymers with Diketopyrrolopyrrole Moieties for High-Performance Field-Effect Transistors. *Adv. Mater.* **2012**, *24*, 4618−4622.
(17) Russell, D. M.; Kugler, T.; Newsome, C. J.; Li, S. P.; Ishida, M.; Shimoda, T. Dedoping of Organic Semiconductors. *Synth. Met.* **2006**, *156*, 769−772.
(18) Hoshino, S.; Yoshida, M.; Uemura, S.; Kodzasa, T.; Takada, N.; Kamata, T.; Yase, K. Influence of Moisture on Device Characteristics of Polythiophene-Based Field-Effect Transistors. *J. Appl. Phys.* **2004**, *95*, 5088−5093.
(19) Wu, F. C.; Cheng, H. L.; Chen, Y. T.; Jang, M. F.; Chou, W. Y. Polymer Bilayer Films with Semi-Interpenetrating Semiconducting/Insulating Microstructure for Field-Effect Transistor Applications. *Soft Matter* **2011**, *7*, 11103−11110.
(20) Hao, X. T.; Hosokai, T.; Mitsuo, N.; Kera, S.; Okudaira, K. K.; Mase, K.; Ueno, N. Control of the Interchain $\pi-\pi$ Interaction and Electron Density Distribution at the Surface of Conjugated Poly(3-hexylthiophene) Thin Films. *J. Phys. Chem. B* **2007**, *111*, 10365−10372.
(21) Arias, A. C.; Endicott, F.; Street, R. A. Surface-Induced Self-Encapsulation of Polymer Thin-Film Transistors. *Adv. Mater.* **2006**, *18*, 2900−2904.
(22) Scaccabarozzi, A. D.; Stingelin, N. Semiconducting: Insulating Polymer Blends for Optoelectronic Applications—A Review of Recent Advances. *J. Mater. Chem. A* **2014**, *2*, 10818−10824.
(23) Babel, A.; Jenekhe, S. A. Morphology and Field-Effect Mobility of Charge Carriers in Binary Blends of Poly(3-hexylthiophene) with Poly[2-methoxy-5-(2-ethylhexoxy)-1,4-phenylenevinylene] and Polystyrene. *Macromolecules* **2004**, *37*, 9835−9840.
(24) Kumar, A.; Baklar, M. A.; Scott, K.; Kreouzis, T.; Stingelin-Stutzmann, N. Efficient, Stable *Bulk* Charge Transport in Crystalline/Crystalline Semiconductor-Insulator Blends. *Adv. Mater.* **2009**, *21*, 4447−4451.
(25) Lee, J.; Jung, J. Y.; Kim, D. H.; Kim, J.-Y.; Lee, B.-L.; Park, J.-I.; Chung, J. W.; Park, J. S.; Koo, B.; Jin, Y. W. Enhanced Electrical Stability of Organic Thin-Film Transistors with Polymer Semiconductor-Insulator Blended Active Layers. *Appl. Phys. Lett.* **2012**, *100*, 083302.
(26) Qiu, L.; Lee, W. H.; Wang, X.; Kim, J. S.; Lim, J. A.; Kwak, D.; Lee, S.; Cho, K. Organic Thin-Film Transistors Based on Polythiophene Nanowires Embedded in Insulating Polymer. *Adv. Mater.* **2009**, *21*, 1349−1353.
(27) Kergoat, L.; Battaglini, N.; Miozzo, L.; Piro, B.; Pham, M.-C.; Yassar, A.; Horowitz, G. Use of Poly(3-hexylthiophene)/Poly(methyl methacrylate) (P3HT/PMMA) Blends to Improve the Performance of Water-Gated Organic Field-Effect Transistors. *Org. Electron.* **2011**, *12*, 1253−1257.
(28) Hamilton, M. C.; Martin, S.; Kanicki, J. Field-Effect Mobility of Organic Polymer Thin-Film Transistors. *Chem. Mater.* **2004**, *16*, 4699−4704.
(29) Paasch, G.; Lindner, T.; Scheinert, S. Variable Range Hopping as Possible Origin of a Universal Relation Between Conductivity and Mobility in Disordered Organic Semiconductors. *Synth. Met.* **2002**, *132*, 97−104.
(30) Kalb, W. L.; Batlogg, B. Calculating the Trap Density of States in Organic Field-Effect Transistors from Experiment: A Comparison of Different Methods. *Phys. Rev. B: Condens. Matter Mater. Phys.* **2010**, *81*, 035327.
(31) Nicollian, E. H.; Brews, J. R. *MOS Physics and Technology*; Wiley: New York, 1981.
(32) Takenobu, T.; Watanabe, K.; Yomogida, Y.; Shimotani, H.; Iwasa, Y. Effect of Postannealing on the Performance of Pentacene Single-Crystal Ambipolar Transistors. *Appl. Phys. Lett.* **2008**, *93*, 073301.
(33) Chiu, L. Y.; Cheng, H. L.; Wang, H. Y.; Chou, W. Y.; Tang, F. C. Manipulating the Ambipolar Characteristics of Pentacene-Based Field-Effect Transistors. *J. Mater. Chem. C* **2014**, *2*, 1823−1829.
(34) Wang, Y. W.; Tseng, G. Y.; Chiu, L. Y.; Lin, B. R.; Lin, Y. Y.; Haung, T. W.; Chou, W. Y.; Horng, L.; Cheng, H. L. Highly Energy-Efficient and Air-Stable Organic Transistors by an Ultrathin Hybrid Dielectric with Large Internal Voltage Generation. *J. Mater. Chem. C* **2014**, *2*, 7752−7760.
(35) Sirringhaus, H.; Brown, P. J.; Friend, R. H.; Nielsen, M. M.; Bechgaard, K.; Langeveld-Voss, B. M. W.; Spiering, A. J. H.; Janssen, R. A. J.; Meijer, E. W.; Herwig, P.; de Leeuw, D. M. Two-Dimensional Charge Transport in Self-Organized, High-Mobility Conjugated Polymers. *Nature* **1999**, *401*, 685−688.
(36) Kline, R. J.; McGehee, M. D.; Kadnikova, E. N.; Liu, J. S.; Frechet, J. M. J.; Toney, M. F. Dependence of Regioregular Poly(3-hexylthiophene) Film Morphology and Field-Effect Mobility on Molecular Weight. *Macromolecules* **2005**, *38*, 3312−3319.
(37) Joshi, S.; Pingel, P.; Grigorian, S.; Panzner, T.; Pietsch, U.; Neher, D.; Forster, M.; Scherf, U. Bimodal Temperature Behavior of Structure and Mobility in High Molecular Weight P3HT Thin Films. *Macromolecules* **2009**, *42*, 4651−4660.
(38) Clark, J.; Chang, F. C.; Spano, F. C.; Friend, R. H.; Silva, C. Determining Exciton Bandwidth and Film Microstructure in Polythiophene Films Using Linear Absorption Spectroscopy. *Appl. Phys. Lett.* **2009**, *94*, 163306.
(39) Wu, F.-C.; Hsu, S.-W.; Cheng, H. L.; Chou, W.-Y.; Tang, F.-C. Effects of Soft Insulating Polymer Doping on the Photovoltaic Properties of Polymer−Fullerene Blend Solar Cells. *J. Phys. Chem. C* **2013**, *117*, 8691−8696.
(40) N'Diaye, M.; Pascaretti-Grizon, F.; Massin, P.; Baslé, M. F.; Chappard, D. Water Absorption of Poly(methyl methacrylate) Measured by Vertical Interference Microscopy. *Langmuir* **2012**, *28*, 11609−11614.

DOI: 10.1021/acsami.5b03864
ACS Appl. Mater. Interfaces 2015, 7, 16486−16494